International Journal of Biological Macromolecules 268 (2024) 131861

Contents lists available at ScienceDirect

International Journal of Biological Macromolecules

journal homepage: www.elsevier.com/locate/ijbiomac

The photophysical, photobiological, and DNA/HSA-binding properties of corroles containing carbazole and phenothiazine moieties

Bruna Matiuzzi Rodrigues [a], Diego Franca de Oliveira [b], Rafael de Queiroz Garcia [b], Otávio Augusto Chaves [c,d], Gabriela Faria Pizzi [e], Luiz Antônio Sodré Costa [e], Leonardo de Boni [b], Bernardo Almeida Iglesias [a,*]

[a] Laboratório de Bioinorgânica e Materiais Porfirínicos, Departamento de Química, Universidade Federal de Santa Maria – UFSM, 97105-900 Santa Maria, RS, Brazil
[b] Instituto de Física, Universidade de São Paulo, Campus São Carlos, CP 369, São Carlos, SP 13560-970, Brazil
[c] CQC-IMS, Departamento de Química, Universidade de Coimbra, Rua Larga, 3004-535 Coimbra, Portugal
[d] Laboratório de Imunofarmacologia, Centro de Pesquisa, Inovação e Vigilância em COVID-19 e Emergências Sanitárias (CPIV), Instituto Oswaldo Cruz (IOC), Fundação Oswaldo Cruz (Fiocruz), Av. Brasil 4036 - Bloco 2, 21040-361 Rio de Janeiro, RJ, Brazil
[e] NEQC – Núcleo de Estudos em Química Computacional, Departamento de Química, ICE, Universidade Federal de Juiz de Fora – UFJF, Campus Universitário s/n, 36036-900 Juiz de Fora, MG, Brazil

ARTICLE INFO

Keywords:
Corroles
Photophysics
Photobiology
DNA-binding
HSA-binding

ABSTRACT

This study characterized four corrole derivatives, namely **Cbz-Cor**, **MetCbz-Cor**, **PTz-Cor**, and **PTzEt-Cor**, examining their photophysical, electrochemical, photobiological, and biomolecule-binding properties. Experimental photophysical data of absorption and emission elements correlated with a theoretical analysis obtained through time-dependent density functional theory (TD-DFT). As for the photophysical properties, we observed lower fluorescence quantum yields and discernible differences between the excited and ground states, as indicated by Stokes shift values. Natural Transition Orbit (NTO) plots presented high occupied molecular orbital - low unoccupied molecular orbital (HOMO-LUMO) densities around the tetrapyrrolic macrocycle in all examples. Our findings demonstrate that corroles maintain stability in solution and offer photostability (<20 %), predominantly in DMSO(5 %)/Tris-HCl (pH 7.4) buffer solution. Furthermore, the singlet oxygen ($^1O_2$) quantum yield and log P_{OW} values underscore their potential application in photoinactivation approaches, as these corroles serve as effective ROS generators with more lipophilic features. We also evaluated their biomolecular binding capacity towards salmon sperm DNA and human serum albumin using spectroscopic techniques and molecular docking analysis for sustenance. Concerning biomolecule interaction profiles, the corrole derivatives showed a propensity for interacting in the minor grooves of the double helix DNA due to secondary forces, which were more pronounced in site III of the human serum protein.

1. Introduction

Corroles are macrocycles found in the porphyrin family, exhibiting unique photophysical and photochemical properties primarily attributed to the C—C connection between adjacent pyrroles. Similar to some porphyrins, they possess low fluorescence quantum yield and high molar extinction coefficient values. The three NH groups in the inner core of each corrolestabilize various metal ions in a high oxidation state [1,2], rendering corroles and/or metallocorroles as potential candidates for photodynamic therapy (PDT) and antimicrobial photodynamic therapy (aPDT) [3–6]. Additionally, these derivatives have been utilized in medicine [7,8], nonlinear optics (NLO) [9,10], and as electroanalytical or photo-responsive [11,12,13] sensors. In terms of photo-processing, corroles are highly light-sensitive, particularly in solution, serving as an efficient photosensitizer. However, they occasionally produce undesirable photo-products [14]. A common strategy to counteract this issue involves using suitable substituents such as penta(fluoro)phenyl groups (C_6F_5) to enhance corrole structure stability.

Free-base corrole and metallocorrole can interact and photocleave biomolecules such as deoxyribonucleic acid (DNA) and human serum albumin (HSA) either through singlet oxygen species ($^1O_2$) for energy transfer mechanisms or radical species (hydroxyl and/or superoxide) for

* Corresponding author.
E-mail address: bernardo.iglesias@ufsm.br (B.A. Iglesias).

https://doi.org/10.1016/j.ijbiomac.2024.131861
Received 3 January 2024; Received in revised form 21 April 2024; Accepted 23 April 2024
Available online 24 April 2024

electron transfer mechanisms [15,16,17]. The reactive oxygen species (ROS) formation and the binding to these biomolecules have been identified as key contributors to photocleavage processes [18,19]. Chromophores like carbazoles and phenothiazines, present in some drugs and dyes, exhibit various biological activities, including neuroleptic, antihistamine, antiviral, and DNA intercalation activities [20,21,22,23]. Consequently, introducing these groups to the corrole's peripheral positions (particularly *meso* positions) can result in the creation of new derivatives with noteworthy photochemical and photobiological properties.

Due to the growing relevance of corroles in PDT applications, this study reports the usage of four literature-related *meso*-mono-substituted corroles with carbazole or phenothiazine units (Fig. 1), namely **Cbz-Cor**, **MetCbz-Cor**, **PTz-Cor**, and **PTzEt-Cor** [24,25]. We conducted their characterization by elemental analysis, HRMS-ESI, and cyclic voltammetry. The photophysical and photobiological properties, including luminescent properties, aggregation, solution stability, photostability, singlet oxygen quantum yield, and water/octanol partition coefficient (log P_{OW}), were also recorded and analyzed. Finally, we also evaluated the biomolecule-binding capacities of these derivatives with DNA and HSA using spectroscopy methods combined with molecular docking calculations.

2. Experimental

2.1. General

All chemical reagents used in this research were of analytical grade, sourced from Sigma-Aldrich® or Oakwood Chemicals®, and required no further purification. To analyze all corroles, we used a PerkinElmer CHN % 2400e equipment for Elemental CHN% analysis. We also analyzed the corroles with a high-resolution micrOTOF QII mass spectrometer equipped with atmospheric pressure chemical ionization in positive mode (Bruker Daltonics, Billerica, USA). To record the mass spectra, we diluted the solutions in methanol (MeOH) to an approximate concentration of 500 ppb, with a flow of 150 μL min^{-1} and capillaries of 3500 V.

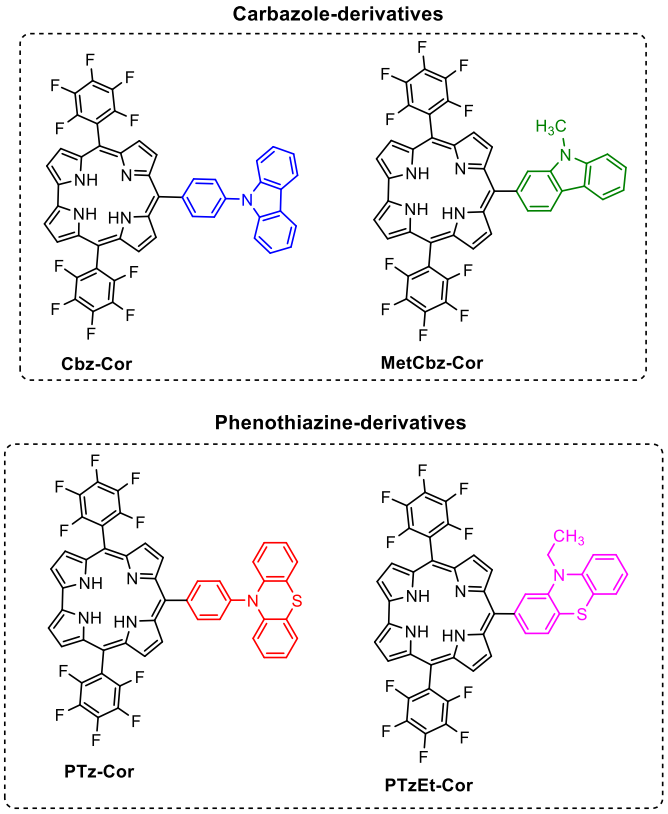

Fig. 1. Chemical structure for the corroles **Cbz-Cor**, **MetCbz-Cor**, **PTz-Cor** and **PTzEt-Cor** under study.

We recorded cyclic voltammograms (CV) with an EcoChemie AutoLab PGSTAT 32 N system under saturated argon in a dry dichloromethane (DCM) solution. We used electrochemical grade tetrabutylammonium hexafluorophosphate ($TBAPF_6$, Sigma-Aldrich®) as the supporting electrolyte at a concentration of 0.1 M. The CV experiments involved a conventional three-electrode system comprised of a glassy-carbon working electrode, platinum wire counter electrode, and another platinum wire functioning as a *pseudo*-reference electrode. To provide an internal reference in DCM, we utilized Ferrocene ($E_{½}$ = 0.40 V) [26]. Readers can find all CV plots in the *Supplementary Information section* — Table S1 and Figs. S1–S4.

Both the salmon sperm double stranded DNA (SS-DNA) and HSA were procured from Sigma-Aldrich®. The albumin is a lyophilized powder that is fatty acid-free and the SS-DNA has low molecular weight, both with a purity ≥99 %.

2.2. Corrole derivatives

The corrole derivatives **Cbz-Cor**, **MetCbz-Cor**, **PTz-Cor,** and **PTzEt-Cor** were synthesized following the method described by Kandhadi, Shivaprasadachary, and their team [24,25]. The derivatives used in these studies were validated through elemental analysis and high-resolution mass spectrometry. *Further details can be found in the Supplementary Information section* —Table S2 and Figs. S2–S5.

2.3. Photophysical analysis

UV–Vis absorption spectra for corroles were obtained at a low molar concentration (≈ 10 μM) in dimethyl sulfoxide (DMSO) to prevent aggregation. These measurements employed a quartz cuvette with a 2.0 mm optical path length and a Shimadzu UV-1800 spectrophotometer. Furthermore, the steady-state fluorescence emission spectra of corroles were measured in a 10 mm quartz cuvette using a Hitachi F7000 fluorimeter, also in DMSO solvent. The sample was maintained at the same low concentration to reduce re-absorption of fluorescence by the corroles.

The fluorescence quantum yields $\left(\phi_f\right)$ for all studied corroles were determined by steady-state fluorescence measurements in a commercial fluorimeter using a 10 cm quartz cuvette. To calculate the ϕ_f values Brouwer's method (Eq. (1)), where hemathoporphyrin IX dissolved in DMSO served as a reference molecule, with ϕ_f = 8.0 % [27,28]. To carry out these measurements and avoid re-absorption of fluorescence by the samples the optical densities were kept at an extremely low level, approximately 0.1. The fluorescence emission spectrum was taken from 550 to 800 nm, and all samples were excited at 520 nm.

$$\phi_f = \phi_f^{ref} \frac{\int_{\lambda_0}^{\lambda} F(\lambda)d\lambda}{\int_{\lambda_0}^{\lambda} F_{ref}(\lambda)d\lambda} \frac{f_{ref}(\lambda)}{f(\lambda)} \frac{n^2}{n_{ref}^2} \quad (1)$$

In this equation, $F(\lambda)$ represents the measured fluorescence spectrum and f signifies the absorbance factor defined as $f = 1 - 10^{A(\lambda_{ex})}$, in which, wherein A is the sample absorbance at the excitation wavelength (λ_{ex} = 520 nm) n is the refractive index of the solvent used identical for both the samples and the reference. The ϕ_f values were discovered to be <5.0 % for all analyzed compounds; these data are presented in Table 1.

To determine the fluorescence lifetime $\left(\tau_f\right)$ of **Cbz-Cor MetCbzCor**, **PTzCor** and **PTzEtCor**, the compounds were dissolved in DMSO and time-resolved fluorescence measurements were taken by exciting the compounds at 515 nm with a 190 femtosecond pulsed laser. The fluorescence decay curves were recorded and analyzed utilizing a mathematical convolution method which employs the instrumental response

Table 1
Photophysical data of studied corroles in DMSO solutions.

Corrole	λ_{abs}, nm (ε; M^{-1} cm^{-1})	λ_{em}, nm	SS (nm/cm^{-1})
Cbz-Cor	291 (58645); 414 (169190); 570 (30055); 609 (22800)	636	27/697
MetCbz-Cor	266 (54105); 416 (169485); 571 (30405); 614 (22450)	646	32/807
Ptz-Cor	279 (85905); 426 (159330); 572 (28145); 612 (22470)	640	28/715
PTzEt-Cor	265 (53715); 415 (169535); 571 (30615); 614 (22455)	652	38/949

Corrole	ϕ_f (%)	τ_f (ns)	k_r (10^7 s^{-1})	ϕ_T (%)	k_{isc} (10^7 s^{-1})	k_{ic} (10^7 s^{-1})
Cbz-Cor	4.40 ± 0.4	3.90 ± 0.4	1.12	7.00	1.80	22.7
MetCbz-Cor	4.20 ± 0.4	3.10 ± 0.3	1.35	42.0	13.6	17.3
Ptz-Cor	2.50 ± 0.3	4.00 ± 0.4	0.62	30.0	7.50	16.9
PTzEt-Cor	4.30 ± 0.4	2.90 ± 0.3	1.48	26.0	9.00	24.0

function of the experiment to fit the decay curve and determine the lifetimes.

Once ϕ_f and τ_f were obtained, we could determine the triplet quantum yield ϕ_T of all corroles by monitoring the fluorescence decay curves Here, a consecutive multiple excitation method, previously described in the literature and already applied in corrole analysis, was used [29,30]. In this method, a pulsed femtosecond laser (190 fs) with an excitation wavelength of 515 nm was used. The measurements in this design were conducted for all the corrole samples dissolved in DMSO. The solutions were prepared in a 20 mm quartz cuvette and measured at a low repetition rate to avoid photo-degradation during measurement. The fluorescence decay curves were obtained for multiple increasing laser intensities to approach a satiation of the first excited singular state population, thus saturating the fluorescence intensity.

Essentially this method engages two pulses, separated in time by about 15 ns to excite the sample at the same volume Consequently, a percentage of the molecules will be transferred to the first singlet excited state From this state, molecules will decay—either returning to the ground state through fluorescence or internal conversion, or, alternatively, being transferred to the triplet state via an intersystem crossing process After approximately 15 ns—the time it takes for the second pulse to arrive at the sample and at the same excited volume—the sample volume will contain fewer molecules in the ground state than before due to the long lifetime of the triplet state [31]. The ratio between the fluorescence intensity induced by the first and the second pulse indicates if the intersystem crossing is happening, and how many of the excited molecules are trapped in the triplet state at this time according to its ϕ_T. With ϕ_T being determined the intersystem crossing time and rate can be calculated.

The following relations can respectively be used: $\tau_{isc} = \tau_f/\phi_T$ and $k_{isc} = 1/\tau_{isc}$. With this information, and the known radiative decay rate ($k_r = \phi_f/\tau_f$), the internal conversion rate (k_{ic}) by using $1/\tau_f = k_r + k_{ic} + k_{isc}$. The aforementioned photophysical parameters are detailed in Table 1. It is important to note that Rhodamine 6G dissolved in ethanol was utilized as a calibration standard for the experimental technique due to its near-zero triplet quantum yield [32], serving as a reference for all the measurements.

2.4. DFT calculations

The study also examined four meso-mono-substituted corroles identified as **Cbz-Cor**, **MetCbz-Cor**, **PTz-Cor**, and **PTzEt-Cor**, utilizing theoretical methodologies. Density Functional Theory (DFT) was employed to optimize and carry out harmonic frequency calculations using the B3LYP/def2-TZVP level of theory [33,34]; all compounds were characterized as ground state species displaying no imaginary frequencies. The dispersion correction was incorporated with the D3BJ keyword [35,36]. The optimization process was conducted in DMSO, using the Continuous Polarizable Model, CPCM [37].

Time-dependent density functional theory (TD-DFT) calculations were performed to acquire more information about the electronic transitions [38]. Both molecular orbitals and the resulting UV–Vis spectra were compared with experimental data. TD-DFT calculations were conducted using the mPWPW/def2-TZVP(−f) level of theory [39]. All calculations were executed with the ab initio Quantum Chemistry *Program* Package, ORCA release 5.0.2, installed on Dell servers at NEQC of the Federal University of Juiz de For a (Brazil) [40,41].

2.5. Aggregation and stability study in solution

To assess the potential aggregation of corroles **Cbz-Cor**, **MetCbz-Cor**, **PTz-Cor**, and **PTzEt-Cor** in solution, absorption spectra were recorded based on the concentration. Pure DMSO or a solvent mixture of DMSO(5 %)/Tris-HCl (pH 7.4) was used. Changes in the λ_{max} from the Soret bands in the UV–Vis spectra were observed in the range of 1.0 to 20 μM.

2.6. Photobiological properties

2.6.1. Photostability

For the photostability assays, corrole derivatives such as **Cbz-Cor**, **MetCbz-Cor**, **PTz-Cor**, and **PTzEt-Cor were freshly prepared** at a concentration of 2.0 μM in both pure DMSO and a DMSO(5 %)/Tris-HCl pH 7.4 buffered mixture. These solutions were stored in the dark at room temperature. The irradiation experiments were conducted over a 30-min period using a white-light LED array system. This system delivered an irradiance of 25 mW/cm^2 and total light dosages of 45 J/cm^2 to 2.0 mL solution samples that were magnetically stirred in cuvettes. The absorbance at the Soret band was measured at 0, 5, 10, 15, 20, 25, and 30 min of irradiation. The results were presented as described in the literature [18].

2.6.2. Water/n-octanol partition coefficients (log P_{OW})

The partition coefficients of corroles, specifically **Cbz-Cor**, **MetCbz-Cor**, **PTz-Cor**, and **PTzEt-Cor**, were determined. These values were obtained using a 3.0 mL volume of *n*-octanol and 3.0 mL of water, as established in the existing literature [30].

2.6.3. Singlet oxygen generation

The generation of singlet oxygen (Φ_Δ) and photo-oxidation constants (k_{po}) were determined as delineated in the literature [42], utilizing typical 1,3-diphenylisobenzofuran (DPBF) photo-oxidation assays. A maximum volume of 1.0 mL, containing 100 μM DPBF in a DMSO solution, was compounded with 0.5 mL (50 μM) of Corroles **Cbz-Cor**, **MetCbz-Cor**, **PTz-Cor**, and **PTzEt-Cor**.

2.7. Biomolecule-binding properties

2.7.1. Binding assays by UV–vis analysis

The binding assays involving corroles **Cbz-Cor**, **MetCbz-Cor**, **PTz-Cor**, and **PTzEt-Cor, tested** with SS-DNA or HSA, were conducted utilizing UV–Vis absorption analysis at a temperature of 298.15 K. These tests were performed in a buffer solution, Tris-HCl pH 7.4, within the 250–800 nm range. A stock solution for each corrole, set at a concentration of 100 μM, was prepared in DMSO. Absorption spectroscopy was employed to determine the nucleic acid pair base concentration for SS-DNA (per base pair at λ = 260 nm) and the amino acid residues concentration derived from HSA (λ = 280 nm). These measurements were facilitated by using the molar extinction coefficients of ε = 7150 M^{-1}

cm^{-1} and ε = 35,700 M^{-1} cm^{-1}, respectively. The titration process involved recording concentrations incrementally which ranged from 0 to 100 μM for both SS-DNA or HSA. The binding constant values (K_b) were then computed based on the Benesi-Hidelbrand equation [43]. Standard Gibb's free-energy (ΔG°) parameters for the compound-biomolecule adduct were also calculated from Kb values, using guidelines provided from available literature [44].

2.7.2. Competitive experiments with DNA:dye by steady-state fluorescence emission

The competitive DNA binding assays were performed using a Horiba FluoromaxPlus fluorimeter. This was accomplished through the successive addition of corroles **Cbz-Cor**, **MetCbz-Cor**, **PTz-Cor**, and **PTzEt-Cor** (from a 100 μM stock solution) to a quartz cuvette containing DNA (10 μM). The cuvette was placed in a pre-treated Tris-HCl buffer solution (pH 7.4) with acridine orange dye (A-T rich specific intercalator; [AO] = 10 μM, λ_{exc} = 480 nm, λ_{em} = 539 nm) or 4′,6-diamidino-2-phenylindole dye (minor groove binder; [DAPI] = 10 μM, λ_{exc} = 359 nm, λ_{em} = 463 nm). The corrole concentrations varied from 0 to 100 μM with all experiments being conducted twice. Steady-state fluorescence emission spectra were observed for DNA:dye adduct after a 2-min incubation period and subsequent additions of the corrole derivative. Calculation of competitive assay constants including the Stern-Volmer quenching constant (K_{SV}), the bimolecular quenching rate constant (k_q), the binding constant (K_b), and Gibb's free energy (ΔG°) were based on the reduction of the steady-state fluorescence emission bands of DNA:dye. The formulas used for these calculations have been previously described in literature [17,44].

2.7.3. Viscosity analysis with DNA

Viscosity analysis was performed using an Ostwald viscometer immersed in a water bath maintained at 298.15 K, as described in the literature [30]. The DNA concentration remained constant throughout all experiments. However, the concentrations of corrole **Cbz-Cor**, **MetCbz-Cor**, **PTz-Cor**, and **PTzEt-Cor** were incrementally increased from 0 to 100 μM in a DMSO(5 %)/Tris-HCl pH 7.4 buffer solution.

2.8. HSA binding assays by fluorescence emission analysis

Cbz-Cor, **MetCbz-Cor**, **PTz-Cor,** and **PTzEt-Cor** exhibited significant absorption at the excitation and emission wavelengths utilized for HSA binding studies; therefore, the inner filter correction was applied to the steady-state fluorescence data in accordance with earlier publications [44]. HSA binding experiments were conducted using corroles (0–100 μM) with HSA (10 μM) and analyzed via steady-state fluorescence emission at 298.15 K in a DMSO (5 %)/Tris-HCl pH 7.4 buffer mixture solution in the 300 to 500 nm range. From these experiments, the Stern-Volmer quenching constant (K_{SV}), bimolecular quenching rate constant (k_q), modified Stern-Volmer constant (K_a), binding constant (K_b), number of binding sites (n), and Gibb's free-energy (ΔG°) values for the quenching assays were calculated according to the Stern-Volmer, modified, and double-logarithmic equations as previously described in the literature [44]. The synchronous fluorescence (SF) spectra, for both HSA (10 μM) absent and present with each corrole, were recorded at 298.15 K. These spectra were recorded in the 240–320 nm range by setting Δλ = 15 nm (for tyrosine residue) and Δλ = 60 nm (for tryptophan residue).

2.9. Time-resolved fluorescence decay with HSA

Lifetime decays (τ_f) were measured using time-correlated single-photon counting (TCSPC) analysis with a DeltaHub controller paired with a Horiba apparatus, using a Ludox® standard solution. Lifetime data was analyzed using DAS6 and Origin® 8.5 software, employing mono-exponential fitting of the raw data. A NanoLED (Horiba) source with 1.0 MHz and a pulse width of <1.2 ns at a 284 nm excitation wavelength served as the excitation source. The concentrations of HSA and each corrole were consistently set at 10 μM in a DMSO (5 %)/Tris-HCl pH 7.4 buffer solution.

2.10. Albumin photo-oxidation by steady-state fluorescence emission analysis

The HSA photo-oxidation assays were carried out using steady-state fluorescence emission at 298.15 K. Stock solutions of HSA (10 μM) were prepared in Tris-HCl buffer (pH 7.4) that contained **Cbz-Cor**, **MetCbz-Cor**, **PTz-Cor**, and **PTzEt-Cor** (each at 10 μM in DMSO; in separate experiments). These solutions were then irradiated with a white-light LED source (with an irradiance of 25 mW/cm^2 and a total light dosage of 30 J/cm^2) for a duration of 20 min. The emission band of the HSA occurred from 0 to 20 min of irradiation, and the photo-oxidation parameters were then calculated according to existing literature [45].

2.11. Molecular docking procedure

The crystallographic structures of DNA and HSA were sourced from the Protein Data Bank with the respective access codes of 1BNA and 1N5U [46,47]. The chemical structures of the fluorinated corroles **Cbz-Cor**, **MetCbz-Cor**, **PTz-Cor**, and **PTzEt-Cor** were constructed and energy-minimized using Density Functional Theory (DFT) in the Spartan 18 software (Wavefunction, Inc., USA) [48].

The molecular docking calculations of the corroles within the biomolecular models were performed utilizing the GOLD 2020.2 software (Cambridge Crystallographic Data Center Software Ltd., UK) [49].

Hydrogen atoms were added to the biomolecules taking into account the tautomeric states and ionization data inferred by the software. The DNA structure reveals two potential binding sites (major and minor grooves) [50,51], whereas the HSA structure displays three primary binding sites located at subdomains IIA, IIIA, and IB—sites I, II, and III respectively [52,53]. The relevant site for each biomolecule was thoroughly investigated in the docking calculations within a 10 Å radius. The exploration procedure allowed for 100,000 genetic operations (crossing, migration, mutation). The ChemPLP scoring function, a default function of the GOLD 2020.2 software [49], was employed. Figures representing the maximum docking score value were generated by the PyMOL Delano Scientific LLC software (Delano Scientific LLC software, Schrödinger, USA) [54].

3. Results and discussion

3.1. Photophysical behavior of free-base corroles

The molar extinction coefficient (solid lines) and steady-state fluorescence emission (dashed lines) spectra of the four corroles (**Cbz-Cor**, **MetCbz-Cor**, **PTz-Cor**, and **PTzEt-Cor**) are illustrated in Fig. 2. These corroles, suspended in DMSO, have Soret bands in the absorption UV–Vis spectra, centering roughly around 420 nm, with a molar extinction coefficient ε of approximately 1.7 × 10^5 M^{-1} cm^{-1}. In addition, their Q-bands span from 500 to 700 nm, associated with an ε of roughly 0.3 × 10^5 M^{-1} cm^{-1}. The emission spectra for all corroles display their maximum at around 650 nm, and the absorption parameters in a DMSO solution are presented in Table 1.

The steady-state fluorescence emission of corroles in DMSO (λ_{exc} near the Soret band, recorded in the 600–800 nm range), along with the photophysical data, are documented in Table 1. The quantum yield values (Φ_f) were computed and, generally, the Φ_f values for the derivatives are remarkably similar across structures. Stokes shifts (SS) were calculated based on the difference between the emission peak and the first Q-band, as these illustrate transitions between identical electronic levels. The SS were discovered to range from 697 to 949 cm^{-1}, indicative of substantial geometric differences between the ground and excited states [55]. The **PTzEt-Cor** molecule exhibits the largest shift,

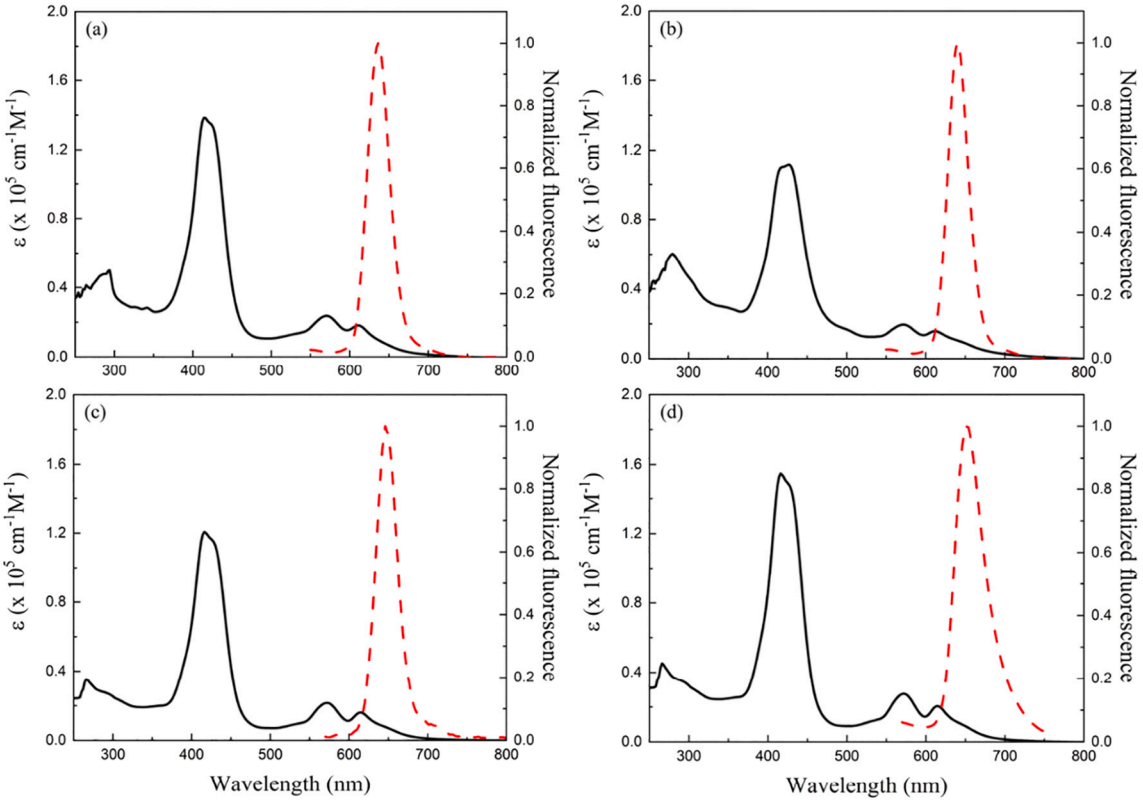

Fig. 2. Molar extinction coefficient (solid line) and normalized fluorescence emission spectra (dashed line) of (a) **Cbz-Cor**, (b) **PTz-Cor**, (c) **MetCbz-Cor**, and (d) **PTzEt-Cor** in DMSO solution.

while **PTz-Cor** has the smallest.

Time-resolved fluorescence revealed that the τ_f values were between 2.9 and 4.0 ns (refer to Table 1). The shortest τ_f (2.9 ns) was noted for **PTzEt-Cor** due to its significant internal conversion (k_{ic}) and intersystem crossing (k_{isc}) rates the longest (4.0 ns) was observed for the **PTz-Cor** molecule which had a lower k_{ic} also having and half the radiative decay (k_r) compared to the other samples. **PTzEt-Cor** and **PTz-Cor** molecules exhibited the highest and lower k_{ic} respectively implying that the highly electronegative sulfur atom and its position in the lateral group profoundly influence the non-radiative energy decay path way.

Considering the SS values for these molecules, it can be inferred that the **PTzEt-Cor** structure facilitates more conformational change upon excitation, resulting in non-radiative energy dissipation. Conversely, **PTz-Cor**, with a more symmetrical lateral group has more restrained movement upon excitation.

The triplet quantum yield values play a significant role in energy dissipation. In the corroles studied, up to $\phi_T = 42\%$ is obtained for **MetCbz-Cor**Nevertheless, internal conversion—known to be the highest rate across all samples—is still the primary energy route, an expected outcome due to the corroles' structural composition.

In comparing the **Cbz-Cor** and **PTz-Cor** compounds—structurally similar except for the addition of a sulfur atom in the phenothiazine moiety—it was observed that the heavier **PTz-Cor** compound had a smaller fluorescence quantum yield and a higher triplet quantum yield formation while maintaining a similar fluorescence lifetime. The corroles **MetCbz-Cor** and **PTzEt-Cor**, both with similar fluorescence lifetime and molecular structure, (the latter incorporating a sulfur atom and a methyl group), showed a comparable radiative rate. However, the intersystem crossing rates showed an increase in the phenothiazine derivative, accompanied by a decrease in the internal conversion rate.

3.2. DFT analysis

All four corroles examined in this study, including Cbz-Cor, MetCbz-Cor, PTz-Cor, and PTzEt-Cor, were subjected to computational analysis. It is initially crucial to consider the geometrical parameters derived from the optimized structure at the potential energy surface's minimum. The shared core element amongst these compounds is the corrole ring. Table 2 presents the primary bond lengths and angles for each compound, while Fig. 3 designates the primary labels aligned with the

Table 2
Main structural parameters for all four corroles. Bond lengths are displayed in Angstroms (Å), angles and torsional angle (dihedral) in degrees (°). Labels are the original ones from the calculations; they appear as stands on Fig. 3.

	Cbz-Cor	MetCbz-Cor	PTz-Cor	PTzEt-Cor
	Bond lengths (Å)			
C22-C57	1.488	1.489	1.488	1.488
C9-C34	1.411	1.412	1.412	1.412
N14-H44	1.025	1.024	1.024	1.024
N14-C9	1.364	1.363	1.362	1.362
N14-C13	1.363	1.361	1.362	1.361
N21···H44	1.785	1.780	1.781	1.778
N21-C16	1.363	1.363	1.362	1.363
N21-C20	1.378	1.378	1.378	1.378
N35-H45	1.006	1.007	1.008	1.008
N35-C34	1.375	1.375	1.376	1.376
N35-C32	1.371	1.371	1.372	1.371
N28-H46	1.007	1.005	1.006	1.006
N28-C27	1.377	1.377	1.376	1.376
N28-C36	1.384	1.384	1.384	1.384
	Torsional angle (dihedral) (°)			
C13-C7-C20	122.7	122.6	122.7	122.6
C16-C22-C27	125.6	125.4	125.7	125.6
C36-C37-C32	122.4	122.6	122.5	122.7
C16-C22-C57-C59	62.2	60.0	61.0	60.1

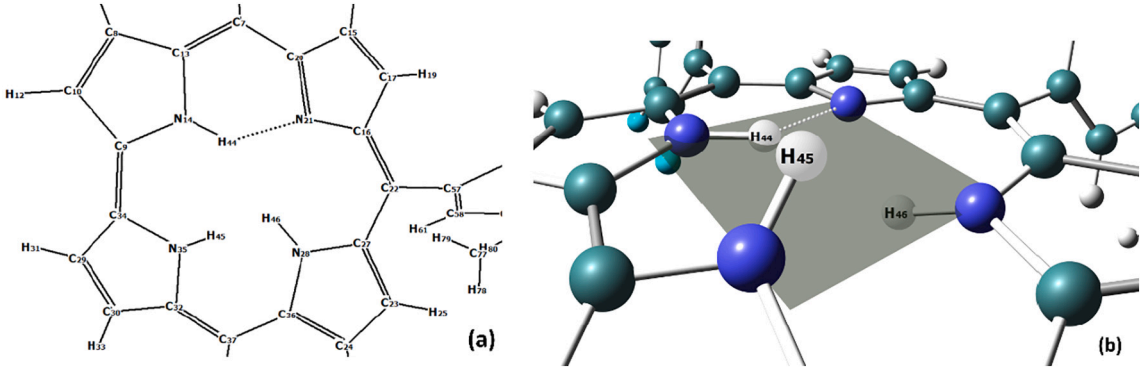

Fig. 3. (a) Schematic view of the corrole ring with the main atoms' labels, according to Table 2. (b) View of the plane formed by all four nitrogen atoms on the corrole ring. It is possible to see H44 in the plane, H45 above and H46 pointing to under the plane.

corrole ring plane.

From the optimized parameters, it is clear that all bond lengths and angles are essentially identical, displaying only negligible variation measured in Angstroms or degrees. This suggests that there is no conformational influence from the meso-substituent even when comparing the carbazole (**Cbz**) and phenothiazine (**PTz**) classes separately. Hydrogen H44 lies in the plane of the nitrogen atoms, forming a hydrogen bond with N21 at an average distance of 1.780 Å. Hydrogen atoms H45 and H46, however, are oriented in opposing directions, indicating different off-plane positions. This is anticipated as the direct C9-C34 bond induces stress in the corrole ring, compelling the pyrrole groups to assume an asymmetrical geometry. Figs. S6 to S9 in the *Supplementary Information section* illustrate all four optimized structures.

A closer examination of the TD-DFT calculations reveals a significant analysis from the frontier molecular orbitals. Table 3 provides the energies, oscillator strengths, electronic transitions, and wavelengths for all corroles studied in this research. The complete theoretical spectra (Figs. S10–S13) and electronic transitions (Tables S3–S6), including the most crucial data, are available in the *Supplementary Information section.*

Examining the corroles spectra (refer to *Supplementary Information section* - Figs. S10–S13), it is evident that the utilized level of theory is satisfactory, as determined by the Soret bands. However, there is a noteworthy shift to higher energies, with a pattern of approximately 20 nm observed in the calculated spectra. Upon considering the comprehensive data provided in Tables S3–S6 (*Supplementary Information section*), it can be observed that the expected transitions are present. These transitions involve a series of narrow band transitions, congruent with the pattern seen in Fig. 2.

Upon reviewing the transitions calculated, they may offer valuable insights about the implicated molecular orbitals. For instance, for **Cbz-Cor,** the primary transition unfolds at 395.6 nm (f = 0.5097), and is attributed to Soret band. For this, two main excitations are involved with four MOs: 217 → 223 and 219 → 225. It is worth noting that the initial transition emerges from the pyrrole ring (lacking NH) to the entire corrole ring, and the subsequent transition from the carbazole unit to the phenyl group and one of the C_6F_5 rings. Analysis of the Soret bands of other compounds reveals some similarities in the transitions, which could generally be classified as π → π* in general.

However, a comprehensive analysis should incorporate the natural transition orbitals (NTO), given the expansive and convoluted contribution from numerous orbitals for each calculated transition. NTO offers a more refined assessment of the molecular orbitals. Once established, Fig. 4 depicts the graphical representation of population analysis derived from NTOs tied to the primary transition mentioned in Table 3. For example, **Cbz-Cor** highlights NTO 221 and NTO 222 as the most representative natural orbitals for the transition calculated at 395.6 nm. It is crucial to clarify that categorizing these orbitals as HOMO and LUMO is misguided, as their significance transcends this designation [56].

Upon examining Fig. 4, it can be observed that all primary transitions for Soret bands initially occur on the corroles rings. In the case of **PTzEt-Cor,** the phenothiazine group has a minor involvement in the natural orbitals. A comprehensive report concerning TD-DFT of corroles is currently under preparation. Our objective is to provide accurate information about these systems and enhance alignment with experimental observations.

Table 3
TD-DFT parameters of studied corroles in DMSO solution at Soret band. Dipole moment in Debye are also included.

Corrole	Main transition	Oscillator strength (f)	λ (nm)	Energy (cm^{-1})	Dipole moment (D)
Cbz-Cor	HOMO−3 → LUMO+3	0.509	395.6	25,277.4	3.740
MetCbz-Cor	HOMO−1 → LUMO+1	0.494	425.9	23,481.2	2.830
PTz-Cor	HOMO−3 → LUMO	0.453	391.4	25,548.0	3.339
PTzEt-Cor	HOMO−2 → LUMO+2	1.058	397.5	25,154.4	5.182

3.3. Solution properties: aggregation studies and stability

The aggregation propensity of corroles **Cbz-Cor**, **MetCbz-Cor**, **PTz-Cor**, and **PTzEt-Cor** in DMSO and DMSO(5 %)/Tris-HCl pH 7.4 buffer solutions was assessed through UV–Vis analysis for potential photobiological applications. The spectral profile for **Cbz-Cor** is depicted in Fig. 5, while the spectral profiles for the remaining corroles are displayed in *Supplementary* Figs. S15–S17. In general, no significant shift in the absorbance of corroles within the tested concentration range (1.0 to 20 μM) was observed, indicating that these compounds do not hinder ROS generation capacity due to their aggregation tendencies. These findings offer promising implications for future PDT application [57].

Regarding solution stability, **Cbz-Cor**, **MetCbz-Cor**, **PTz-Cor**, and **PTzEt-Cor** demonstrated chemical stability in DMSO over a period of 3 days. No spectral alterations or emergence of new transition bands were noted, indicating the non-decomposition of the studied corroles in the solution during this time frame (refer to *Supplementary* Figs. S18–S21).

3.4. Photobiological parameters

3.4.1. Photostability behavior

Generally, corroles exhibit instability when subjected to prolonged light exposure, causing photo-bleaching, which can be analyzed to evaluate potential photo-degradation of the tetrapyrrole ring following light dosage irradiation. Changes observed in the absorption spectra of

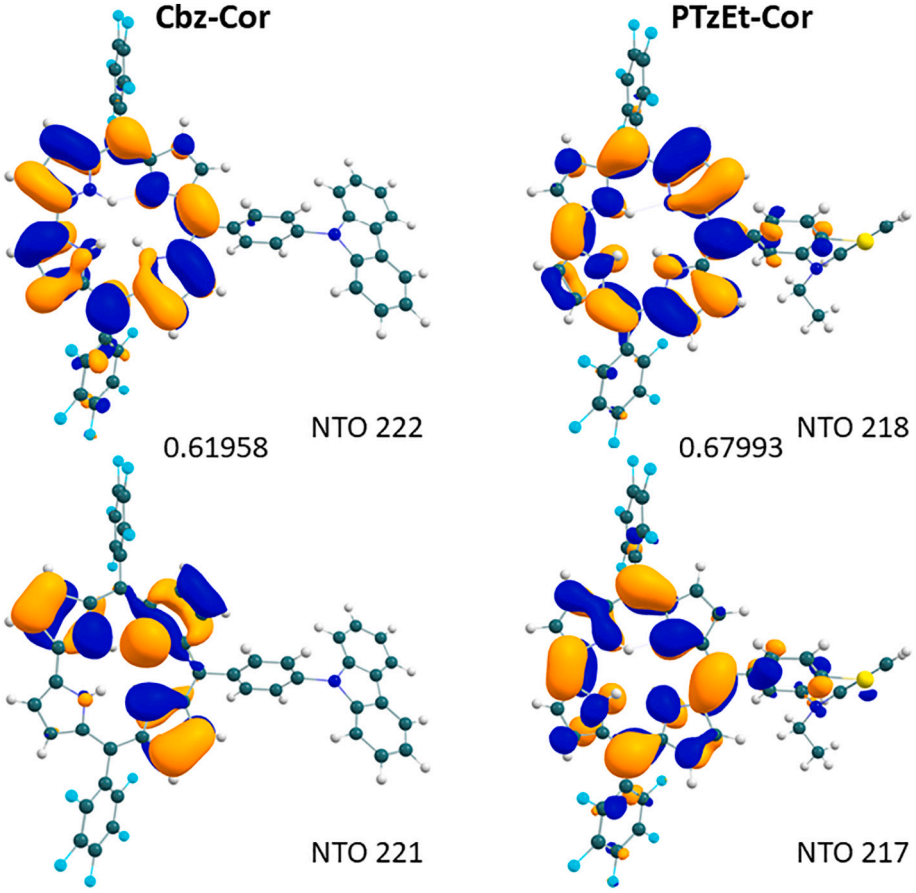

Fig. 4. Natural transition orbitals (NTO) plots for **Cbz-Cor** and **PTzEt-Cor** examples in DMSO. The occupation number for each NTO pair has been given.

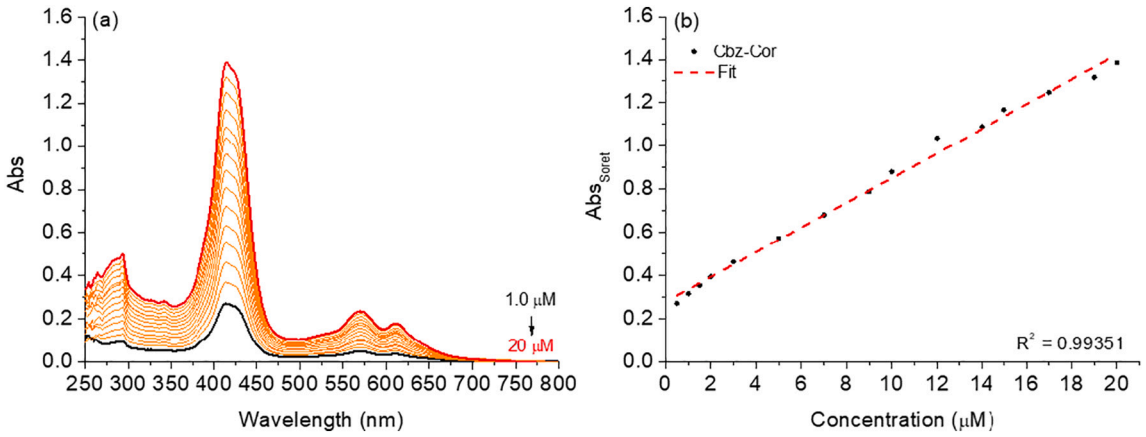

Fig. 5. (a) Aggregation analysis for **Cbz-Cor**, using DMSO as solvent and (b) Abs_{Soret} versus concentration.

Cbz-Cor, **MetCbz-Cor**, **PTz-Cor**, and **PTzEt-Cor** over time demonstrated that the corroles had a decent degree of photostability when exposed to a white-light LED array system with a capacity of 25 mW/cm^2 (total light dosages of 45 J/cm^2) for 30 min in DMSO or DMSO(5 %)/Tris-HCl pH 7.4 buffer solutions (Fig. 6). The photo-degradation constants (k_{pd}) for corroles were ascertained and tracked at the Soret band during irradiation, with the findings summarized in Table 4.

3.4.2. *Singlet oxygen ($^1O_2$) production and log P_{OW}*

The ability of the studied corroles to produce $^1O_2$ species was observed using the 1,3-diphenylisobenzofuran (DPBF) method in a DMSO solution. The literature previously evaluated the generation of $^1O_2$ in DMSO by the standard **TPhCor** corrole [18]. The photo-oxidation constant (k_{po}) and singlet oxygen quantum yield (Φ_Δ) for corroles **Cbz-Cor**, **MetCbz-Cor**, **PTz-Cor**, and **PTzEt-Cor** are documented in Table 4, while all DPBF photo-oxidation spectra can be found in the *Supplementary Information section* (Figs. S22–S25). As noted, the calculated Φ_Δ values for the standard TPhCor corrole lacking C_6F_5 and heterocycle peripheral groups appear to be lower than all the other corrole structures under study (Table 4). This discrepancy could be attributed to potential triplet population and the deactivation of the first excited-state via internal conversion (IC) pathways, likely as a result of the presence of the carbazole or phenothiazine moiety. Consequently, derivatives of carbazole and phenothiazine corroles display potential for photo-

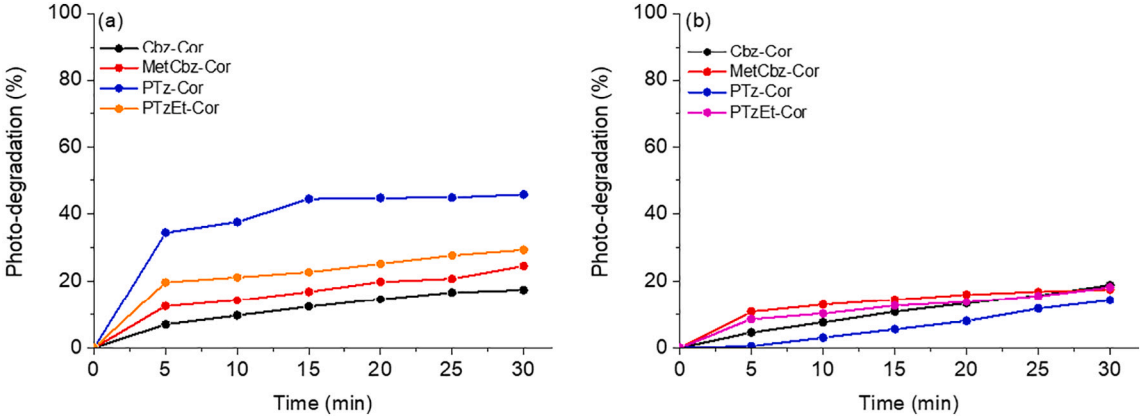

Fig. 6. Photostability assays of corroles at white-light LED irradiation for 30 min in (a) DMSO and (b) DMSO(5 %)/Tris-HCl pH 7.4 buffer solutions.

Table 4
Photo-bleaching (k_{pb}) constant, DPBF photo-oxidation (k_{po}) constant, and singlet oxygen quantum yields (Φ_Δ) of studied corroles.

	Photo-degradation		Photobiological parameters		
Corrole	k_{pb} (min^{-1})[a]	k_{pb} (min^{-1})[b]	k_{po} (M^{-1} s^{-1})	Φ_Δ (%)	log P_{OW}[d]
Cbz-Cor	0.010	0.006	0.450	49.0	+2.38
MetCbz-Cor	0.014	0.013	0.460	50.0	+1.91
PTz-Cor	0.041	0.005	0.230	30.0	+2.23
PTzEt-Cor	0.020	0.010	0.220	29.0	+2.29
TPhCor	0.025[c]	0.019[c]	0.165[c]	16.0[c]	+2.67

[a] In DMSO solution.
[b] In DMSO(5 %)/Tris-HCl pH 7.4 buffer solution.
[c] **TPhCor** = *meso*-tri(phenyl)corrole [18].
[d] In *n*-octanol/water mixture.

oxidation processes once exposed to light irradiation in the presence of oxygen. Furthermore, in terms of the partition coefficients (log P_{OW}) of the corroles in a *n*-octanol/water mixture, the recorded positive log P_{OW} values align with existing literature, thus indicating increased lipophilic behavior of these compounds [30].

3.5. Interactive assays with biomolecules

3.5.1. Biomolecule-binding properties by UV–vis assays

The corroles studied (**Cbz-Cor**, **MetCbz-Cor**, **PTz-Cor**, and **PTzEt-Cor)** were titrated with increasing concentrations of biomolecules (DNA or HSA), and the corresponding absorption spectra were measured. Fig. 7 illustrates the absorption spectra for **PTz-Cor** both without and in the presence of escalating biomolecule concentrations. The absorption profiles for the other corroles are available in the *Supplementary Information section* (Figs. S26–S31). Data for hypo- or hyperchromism (*H*%), red-shift (Δλ), binding constant (K_b), and Gibb's binding free-energy (ΔG) in the presence of either DNA or HSA are summarized in Table 5. Given that the K_b values are roughly 10^4 M^{-1}, it suggests that the corroles under study possess a relatively strong binding affinity towards DNA. This observation aligns with findings reported in the literature for other corroles [17,30,58].

Regarding protein binding, the K_b values are slightly lower than those for DNA (at approximately 10^3 M^{-1}), hinting that these corroles may prefer to interact with nucleic acids, likely through the formation of corrole:DNA adducts via secondary interactions and possible insertion of the corroles into DNA grooves. The experimental free-energies were determined to be negative values (ΔG; in kJ mol^{-1}), indicating the spontaneous nature of the interaction between the corroles and the biomolecules. This mode of interaction with DNA and HSA was also supported by molecular docking calculations (see Section 3.5.6).

3.5.2. Competitive corrole:dye:DNA assays by steady-state fluorescence measurements

To confirm the binding capacity and the primary region where the corroles **Cbz-Cor**, **MetCbz-Cor**, **PTz-Cor**, and **PTzEt-Cor** interact with DNA structure, we conducted competitive binding assays that utilized steady-state fluorescence quenching measurements to displace the commercial intercalating acridine orange (AO) and minor groove binder 4′,6-diamidino-2-phenylindole (DAPI) [58]. We observed changes in the dye-DNA fluorescence emission spectra in the presence of corroles, using a fixed DNA concentration pre-treated with the selected dye, both before and after successive corrole additions.

As illustrated in Fig. 8a, for the selected corrole **MetCbz-Cor**, dye-DNA adducts exhibited potent emission at 539 nm when excited at 480 nm (for AO-DNA), while for DAPI-DNA adducts excited at 359 nm, the maximum emission was at 463 nm (Fig. 8c). The steady-state fluorescence emission spectra for the other corroles and DNA-dyes are presented in the *Supplementary Information section* (Figs. S32–S37).

For AO intercalator dye (specific A-T-rich), the gradual addition of MetCbz-Cor to the AO:DNA adduct **resulted in fluorescence quenching** (Fig. 8a). The decrease in the AO:DNA adduct emission intensity in the presence of corroles and Stern-Volmer quenching (K_{SV}) values of approximately 10^3 M^{-1} suggest a moderate interactive profile, which correlates well with the absorption DNA parameters previously detailed in Table 5. Based on these observations, we employed the same methodology with DAPI dye to determine whether the studied compounds potentially interact via grooves (Fig. 8c). Similar to the AO:DNA experiment, a significant fluorescence quenching was noted upon adding the corroles. Considering the K_{SV} and binding constant (K_b) values obtained for the DAPI:DNA adducts, a greater affinity for interaction via the minor groove than intercalation was apparent.

Two potential mechanisms can explain the observed fluorescence quenching: a static process (via ground-state association) or a dynamic process (collisional interaction). These processes occur as the corroles **Cbz-Cor**, **MetCbz-Cor**, **PTz-Cor**, and **PTzEt-Cor** can interact with the grooves of DNA, primarily via the minor groove. As depicted in Table 6, the rate constant (k_q) values are approximately 10^{12} M^{-1} s^{-1}, three orders of magnitude larger than the diffusion rate constant ($k_{diff} \approx 7.40 \times 10^9$ M^{-1} s^{-1}, at 305 K) [59], suggesting a likely static nature of the interaction. Finally, variances in K_{SV} and K_b values can be ascribed to a preference for interaction via the minor groove, rather than by intercalation. This finding corroborates those obtained from UV–Vis and subsequent molecular docking calculations.

3.5.3. HSA-binding analysis by steady-state fluorescence experiments

Fluorescence emission spectroscopy is a technique extensively used for determining experimental binding parameters between albumins and small endogenous and exogenous compounds. When excited at 295 nm, the HSA exhibits a maximum fluorescence emission peak near 334

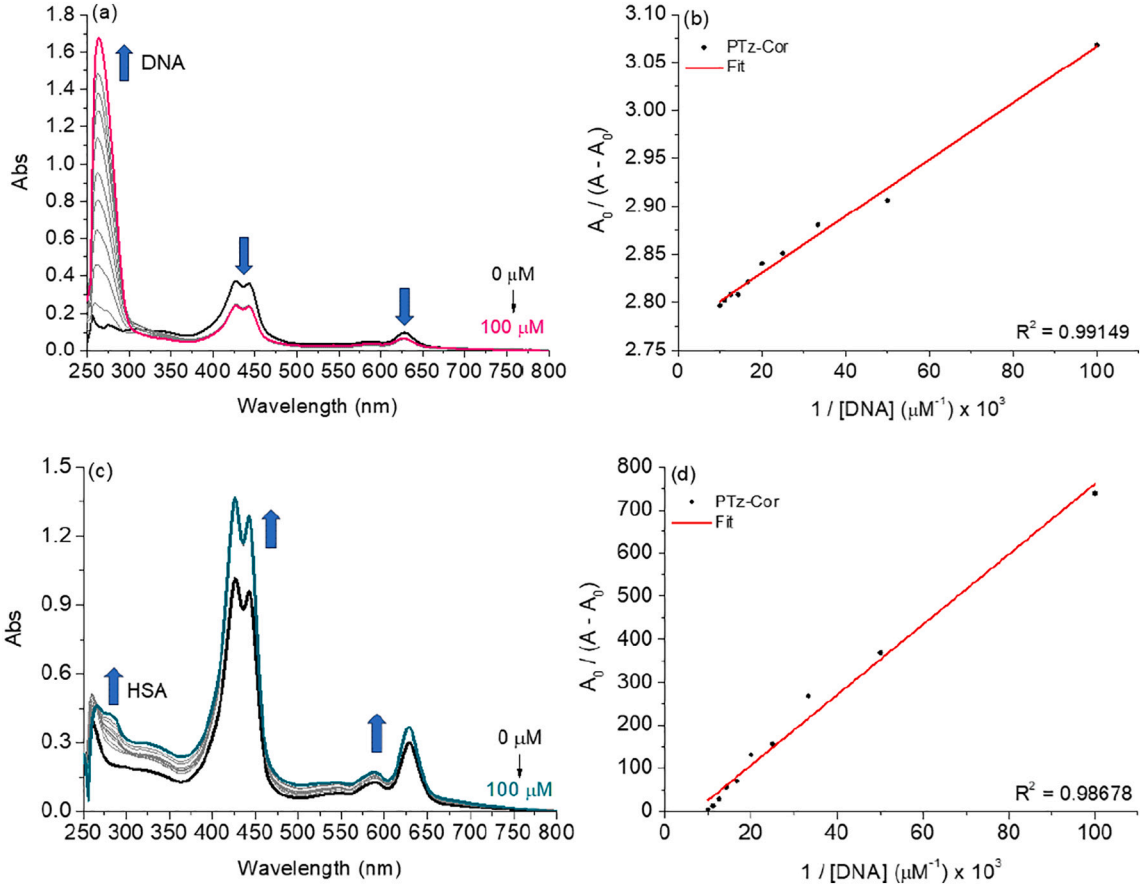

Fig. 7. Absorption UV–Vis spectra analysis of (a) DNA and (b) HSA interaction in the presence of **PTz-Cor** without and in the presence of successive additions of biomolecules ranging from 0 to 100 μM in DMSO(5 %)/Tris-HCl pH 7.4 buffer solution.

Table 5
Binding interactive parameters between DNA/HSA and corroles **Cbz-Cor**, **MetCbz-Cor**, **PTz-Cor**, and **PTzEt-Cor** by UV–Vis analysis in DMSO(5 %)/Tris-HCl pH 7.4 buffer solution.

	DNA			
Corrole	*H*(%)[a]	Δλ (nm)[b]	K_b (M^{-1})[c] × 10^4	ΔG° (kJ/mol)[d]
Cbz-Cor	11.35	0.0	1.44 ± 0.12	−23.75
MetCbz-Cor	9.45	0.0	0.57 ± 0.04	−21.45
PTz-Cor	35.75	0.0	3.39 ± 0.03	−25.85
PTzEt-Cor	41.10	0.0	2.23 ± 0.06	−24.80

	HSA			
Corrole	*H*(%)[a]	Δλ (nm)[b]	K_b (M^{-1})[c] × 10^4	ΔG° (kJ/mol)[d]
Cbz-Cor	20.0	0.0	3.93 ± 0.55	−20.50
MetCbz-Cor	17.0	0.0	0.47 ± 0.03	−15.25
PTz-Cor	26.0	0.0	0.12 ± 0.02	−11.85
PTzEt-Cor	27.0	0.0	0.14 ± 0.02	−12.25

[a] Hypo or hyperchromism: Soret band = $Abs_{initial} - Abs_{final} / Abs_{initial} \times 100$ %.
[b] Red shift.
[c] Binding constant.
[d] Gibb's free energy, obtained using gas constant $R = 8.314$ J/K.mol and temperature $T = 298.15$ K.

nm as a result of the tryptophan fluorophore residue. For instance, Fig. 9 illustrates the emission spectra of albumin without and with successive additions of MetCbz-Cor (ranging from 0 to 100 μM) at 298.15 K. The fluorescence emission spectra for additional corrole derivatives are provided in the *Supplementary Information section* (Figs. S38-S40). Upon successive additions of the selected corrole, fluorescence quenching behavior is observed without any significant hypso- or bathochromic shifts, suggesting that the corrole interacts with the tryptophan residue without altering the fluorophore's microenvironment.

To assess the primary fluorescence quenching mechanism induced by corroles, the Stern–Volmer equation was employed. The K_{SV} and k_q values for the interaction between HSA and the corroles under investigation are presented in Table 7. In these experiments, moderate K_{SV} values were found for both corrole systems, implying that they can interact with the albumin's binding site, which contains a tryptophan residue, with a moderate capacity (≈10^3 M^{-1}). The observed k_q values are approximately three orders of magnitude higher (10^{12} M^{-1} s^{-1}) than the diffusion rate constant (k_{diff} approximately equal to 7.40 × 10^9 M^{-1} s^{-1}), confirming that the main fluorescence quenching mechanism is a static process (ground-state association) [59].

The modified Stern-Volmer constant (K_a) for each corrole is in the order of 10^3 M^{-1}, indicative of moderate interaction capacity (Table 7), corroborating the K_{SV} values. Moreover, the K_b values obtained through the double logarithmic equation (another mathematical approach to evaluate binding capacity) are also in the order of 10^3 M^{-1}, suggesting a moderate binding capacity between HSA and corroles (Table 7). The presence of the methyl-carbazole moiety in the corrole periphery of **MetCbz-Cor** introduces minor fluctuations in the K_a and K_b values, slightly increasing the binding capacity.

Furthermore, the number of binding sites (*n*) for the corroles under study is summarized in Table 7, implying that the presence of different moieties (phenothiazine or carbazole) does not affect the HSA:corrole ratio. In other words, one molecule of corrole can bind to one protein molecule (1:1 ratio). Lastly, the negative ΔG values observed indicate

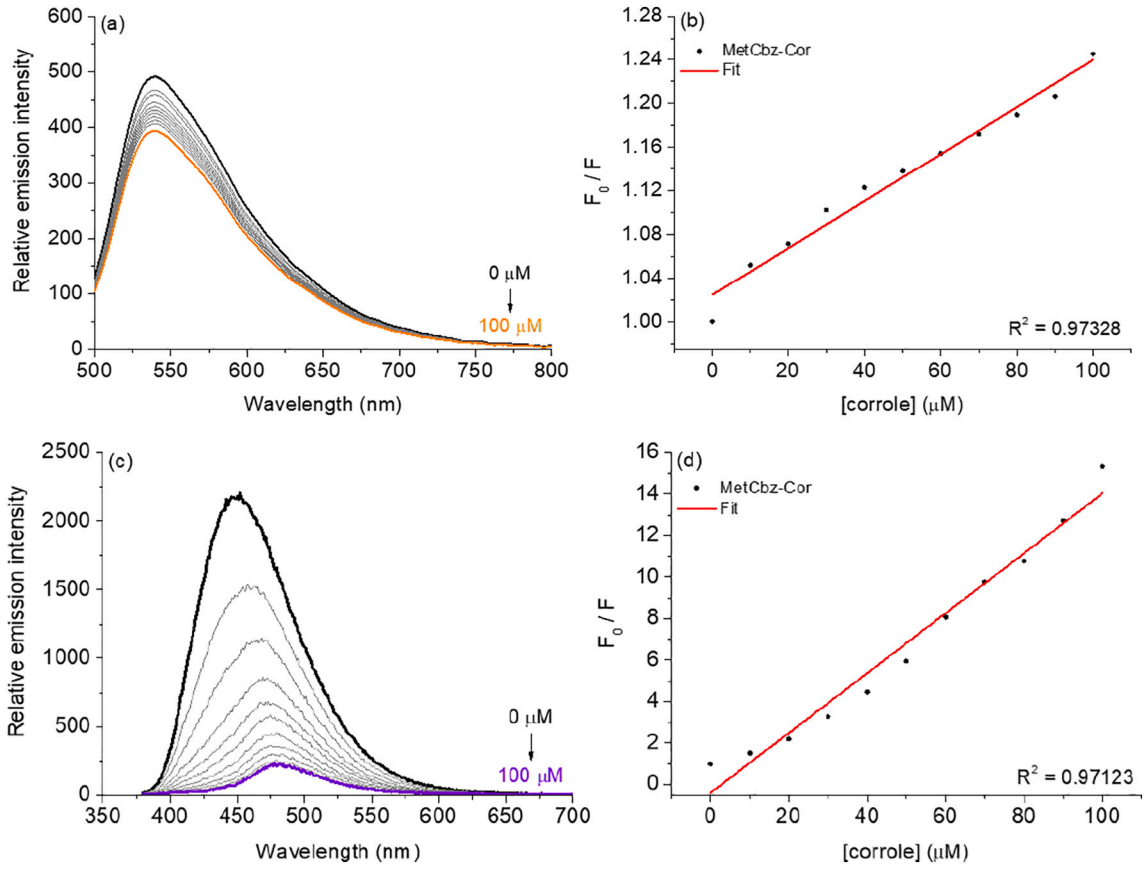

Fig. 8. Steady-state fluorescence emission spectra for the competitive assays in the presence of (a) AO-DNA and (c) DAPI-DNA before and upon successive additions of **MetCbz-Cor**, ranging from 0 to 100 μM in DMSO(5 %)/Tris-HCl pH 7.4 buffer solution. (b, d) The corresponding Stern-Volmer plots.

Table 6
Competitive binding parameters between DNA:dye and corroles by steady-state fluorescence emission, where: AO = Acridine Orange dye (A-T-rich intercalator) and DAPI = 4′,6-diamidino-2-phenylindole (minor groove binder).

	AO:DNA				
Corrole	Q (%)[a]	K_{SV} (M^{-1}) × 10^3	k_q (s^{-1} M^{-1}) × 10^{11}[b]	K_b (M^{-1}) × 10^3	ΔG (kJ/mol)[d]
Cbz-Cor	9.10	0.97 ± 0.02	5.70 ± 0.16	0.26 ± 0.13	−13.80
MetCbz-Cor	19.70	2.15 ± 0.06	12.6 ± 0.50	0.20 ± 0.10	−13.15
PTz-Cor	11.75	1.18 ± 0.02	6.95 ± 0.16	0.79 ± 0.10	−16.55
PTzEt-Cor	30.20	3.92 ± 0.08	23.0 ± 0.66	3.16 ± 0.24	−20.00

	DAPI:DNA				
Corrole	Q (%)[a]	K_{SV} (M^{-1}) × 10^4	k_q (s^{-1} M^{-1}) × 10^{12}[c]	K_b (M^{-1}) × 10^3	ΔG (kJ/mol)[d]
Cbz-Cor	30.6	0.34 ± 0.03	0.15 ± 0.25	3.91 ± 0.05	−20.50
MetCbz-Cor	96.0	14.4 ± 0.04	65.4 ± 0.33	81.6 ± 0.05	−28.00
PTz-Cor	45.9	0.85 ± 0.01	3.86 ± 0.08	42.3 ± 0.12	−26.50
PTzEt-Cor	53.3	1.10 ± 0.02	5.00 ± 0.16	49.0 ± 0.09	−26.80

[a] $Q(\%) = Em_{initial} - Em_{final} / Em_{initial} \times 100$.
[b] AO:DNA lifetime ($\tau_f = 1.70$ ns).
[c] DAPI:DNA lifetime ($\tau_f = 2.20$ ns).
[d] Using $R = 8.3145$ J/mol. K and $T = 298.15$ K.

the spontaneity of the interaction (Table 7). Further information on the binding capacity between HSA and corroles will be discussed in the molecular docking calculations section.

3.5.4. HSA lifetime study

Time-resolved fluorescence decays (as shown in Fig. S41 in the *Supplementary Information section*) were executed to further validate the principal fluorescence quenching mechanism for the interaction between HSA and corroles. The fluorescence lifetime (τ_f) in a DMSO(5 %)/Tris-HCl pH 7.4 buffer solution of free HSA and HSA bound with corroles **Cbz-Cor**, **MetCbz-Cor**, **PTz-Cor**, and **PTzEt-Cor** exhibited significant fluctuations (refer to Table 8). Contrary to the steady-state fluorescence quenching analysis, the time-resolved decays were obtained by excitation at 284 nm, indicating the potential impact of the excitation mode on the primary fluorescence quenching mechanism. In other words, the results from the steady-state analysis showing a predominance of static behavior (where the Trp residue is selectively excited) were not mirroring those from the time-resolved analysis. The latter indicated a contribution from the dynamic process, which excited both the Trp, Tyr, and Phe residues. Thus, the test compounds are not only interacting in the cavity housing the Trp residue but also in regions rich in phenylalanine or tyrosine residues. They could even interact in a cavity near the Trp residue, such as subdomain IB (site III), which will be scrutinized in future molecular docking calculations.

3.5.5. Photo-oxidation of HSA induced by corroles

The HSA is susceptible to photo-oxidative processes primarily due to ROS, such as singlet oxygen ($^1O_2$), hydroxyl (•OH), superoxide ($O_2^{\bullet -}$), and hydroperoxyl (•OOH) radical species. The efficiency of photo-oxidation of **Cbz-Cor**, **MetCbz-Cor**, **PTz-Cor**, and **PTzEt-Cor**, in oxidizing HSA solution, was evaluated using a white-light LED

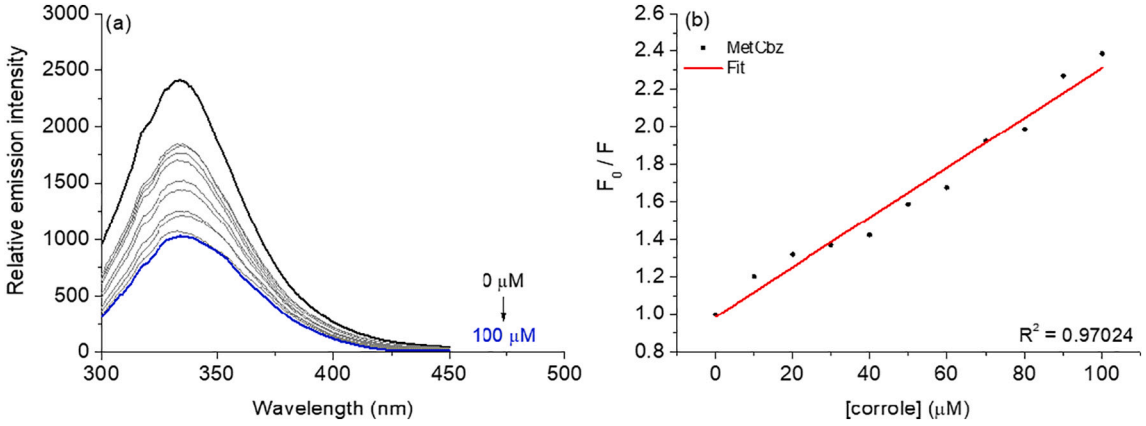

Fig. 9. Steady-state fluorescence emission spectra for (a) HSA:**MetCbz-Cor** and (b) the Stern-Volmer plot at 298.15 K (λ_{exc} = 290 nm). [HSA] = 10 μM and [corroles] = 0 to 100 μM range.

Table 7
Binding parameters for the HSA:corroles interaction at 298.15 K in DMSO(5 %)/Tris-HCl pH 7.4 buffer solution.

Corrole	*Q*(%)[a]	K_{SV} (M^{-1})[b] x 10^3	k_q (M^{-1} s^{-1})[c] x 10^{12}	K_a (M^{-1})[d] x 10^3	K_b (M^{-1})[e] x 10^3	*n*[f]	ΔG (kJ/mol)[g]
Cbz-Cor	17.0	1.98 ± 0.04	0.35 ± 0.33	1.93 ± 0.63	3.25 ± 0.18	1.00 ± 0.04	−20.05
MetCbz-Cor	57.0	13.2 ± 0.04	2.33 ± 0.33	10.5 ± 0.11	9.20 ± 0.08	0.95 ± 0.08	−22.60
PTz-Cor	33.0	4.85 ± 0.01	2.33 ± 0.08	7.12 ± 0.10	3.26 ± 0.18	0.90 ± 0.04	−20.05
PTzEt-Cor	40.0	6.70 ± 0.02	1.18 ± 0.16	8.39 ± 0.26	3.50 ± 0.27	0.95 ± 0.06	−20.20

[a] Quenching (%) = (F_0 − F) / F_0 × 100.
[b] Stern-Volmer quenching constant.
[c] Bimolecular quenching rate constant obtained by τ_0 = 5.67 ns.
[d] Modified Stern-Volmer binding constant.
[e] Double logarithmic binding constant.
[f] Number of binding sites.
[g] Gibb's free energy, when gas constant *R* = 8.3145 J/mol K^{-1} and temperature *T* = 298.15 K.

Table 8
Fluorescence lifetime parameter for HSA without and in the presence of corroles in DMSO(5 %)/Tris-HCl pH 7.4 buffer solution.

	τ_f (ns)	χ^2
HSA	5.26 ± 0.020	1.13555
HSA:Cbz-Cor	4.95 ± 0.011	1.18795
HSA:MetCbz-Cor	5.01 ± 0.030	0.94895
HSA:PTz-Cor	5.51 ± 0.033	1.15930
HSA:PTzEt-Cor	5.50 ± 0.022	1.01830

irradiation source at an irradiance of 25 mW cm^{-2} and total light dosages of 30 J cm^{-2}, both in the absence and presence of fixed concentrations of corroles under study. The fluorescence emission spectra for all these are provided in the *Supplementary Information section* (Figs. S42–S46).

Table 9 presents the data for fluorescence quenching (*Q*%) observed in HSA when exposed to the selected corroles under 20 min of irradiation. Without the corroles, there was no observable photo-oxidation of the biomolecule even after the designated irradiation period (data not included). The results suggest that under white-light illumination, the **Cbz-Cor** corrole exhibits a higher photo-degradation constant (k_{pd}) (Table 9), indicating superior photo-oxidation values compared to compounds containing phenothiazine. This could be attributed to the increased generation of ROS, specifically singlet oxygen species, in corroles incorporating the carbazole fragment.

Table 9
The HSA photo-oxidation analysis with studied corroles in DMSO(5 %)/Tris-HCl pH 7.4 buffer solution, at white-light LED irradiation conditions (25 mW cm^{-2} and 30 J cm^{-2}; 20 min.).

Corrole	*Q* (%)[a]	k_{po} (min^{-1})[b]
Cbz-Cor	18.0	0.0162
MetCbz-Cor	13.0	0.0087
PTz-Cor	7.50	0.0055
PTzEt-Cor	14.0	0.0114

[a] Quenching = *Q*(%) = F_0 − F / F_0 × 100 %.
[b] First-order kinetics profile.

3.5.6. *Molecular docking calculations*

The experimental data revealed that all fluorinated corroles under study could interact with DNA and HSA. Therefore, molecular docking calculations were performed to provide an atomic-level explanation of the binding capacity, suggest the primary interactive region, and identify the intermolecular forces responsible for stabilizing the biomolecule-ligand complex. Table 10 displays the docking score values for the DNA-corrole and HSA-corrole interactions at the feasible binding sites identified. As the docking score value is higher for interaction with DNA in the minor groove (69.51) than the major groove (44.17), as exemplified by the DNA:Cbz-Cor interaction, this suggests that the corroles might interact predominantly with DNA via the minor groove.

Table 10
Molecular docking score values (dimensionless) for the interaction between DNA/HSA and corroles.

	DNA		HSA		
Sample	Minor Groove	Major Groove	Site I	Site II	Site III
Cbz-Cor	69.51	44.17	51.44	61.94	85.20
MetCbz-Cor	66.12	40.49	63.16	37.86	70.22
PTz-Cor	67.40	45.30	41.51	53.67	58.03
PTzEt-Cor	71.88	42.71	39.07	38.99	83.13

This conclusion aligns with the experimental dye displacement data. According to previous literature, various corroles, such as fluorinated *meso*-C_6F_5-corroles such as 5,15-bis(pentafluorophenyl)-10-(phenyl)corrole and 5,15-bis(pentafluorophenyl)-10-(1-pyrenyl)corrole [17], displayed the same in silico trend.

Nevertheless, molecular docking score values in HSA studies suggest that Cbz-Cor, PTz-Cor, PTzEt-Cor, and MetCbz-Cor predominantly interact with subdomain IB (site III) of the albumin structure. This subdomain is exposed to the aqueous media. Likely, the corroles under study preferentially bind in this protein pocket due to the high steric volume of the ligand structure. This volume could affect the likelihood of the corroles becoming embedded in more internal sites. According to the literature, some fluorinated corroles [17] and porphyrins, including protoporphyrin IX [47], *meso*-tetra(4-pyridylvinylphenyl)porphyrins [60], and peripheral Pt(II) derivatives on a tetra-cationic(4-pyridyl) porphyrin [61], display the same in silico trend.

Figs. 10 and 11 illustrate the optimal docking pose for the interaction between DNA (minor groove) or HSA (site III) and the corroles under study. Additionally, Tables S7 and S8 in the *Supplementary Information section* delineate the primary nitrogenous bases for DNA or amino acid residues for HSA, along with the intermolecular forces and distances involved in the interaction process. Molecular docking results indicate hydrogen bonding and van der Waals interactions as the primary intermolecular forces in the binding with both biomolecules. For

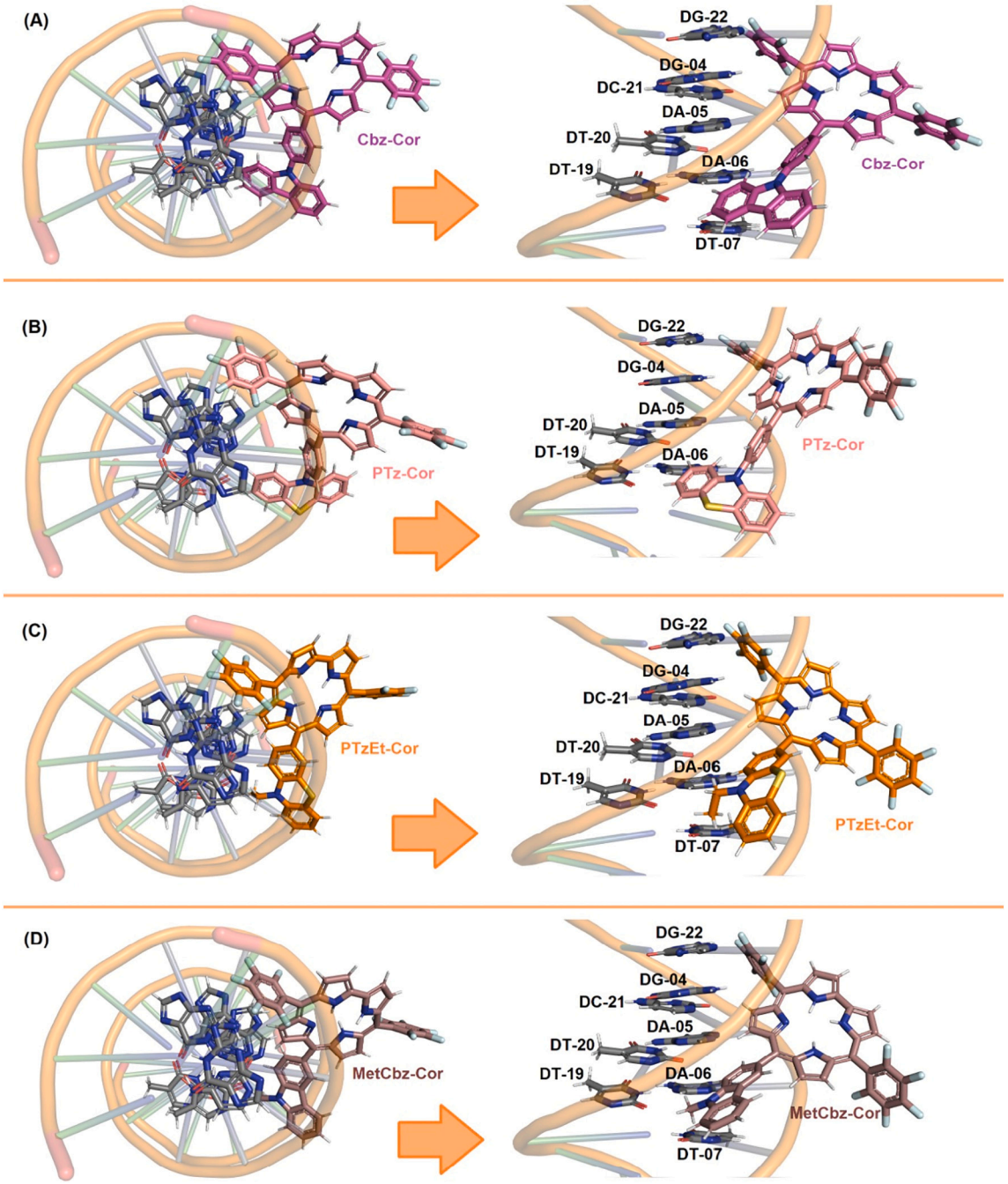

Fig. 10. Best docking pose (*ChemPLP* function) for the interaction between (A) DNA:**Cbz-Cor**, (B) DNA:**PTz-Cor**, (C) DNA:**PTzEt-Cor**, and (D) DNA:**MetCbz-Cor** in the minor groove. Selected nitrogenated bases are in stick representation in gray color, while **Cbz-Cor**, **PTz-Cor**, **PTzEt-Cor**, and **MetCbz-Cor** are represented in pink, beige, orange, and brown color, respectively. Elements' color: hydrogen: white, oxygen: red, fluor: cyan, and nitrogen: dark blue. (For interpretation of the references to color in this figure legend, the reader is referred to the web version of this article.)

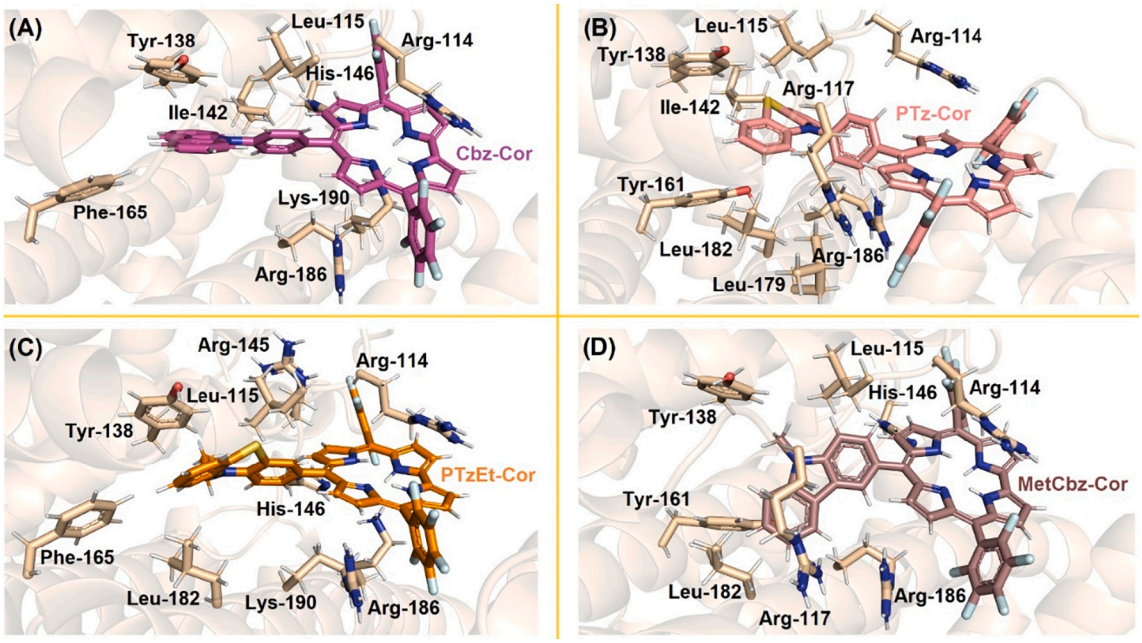

Fig. 11. Best docking pose for the interaction between (A) HSA:**Cbz-Cor**, (B) HSA:**PTz-Cor**, (C) HSA:**PTzEt-Cor**, and (D) HSA:**MetCbz-Cor** in the site III. Selected amino acid residues, **Cbz-Cor**, **PTz-Cor**, **PTzEt-Cor**, and **MetCbz-Cor** are represented in light orange, pink, beige, orange, and brown color, respectively. Elements' color: hydrogen: white, oxygen: red, fluor: cyan, and nitrogen: dark blue. (For interpretation of the references to color in this figure legend, the reader is referred to the web version of this article.)

instance, the molecular docking results for the DNA:**Cbz-Cor** interaction suggest that the hydrogen from the amine group of DG-04 and DG-22 potentially acts as a donor for hydrogen bonding with the fluorine atoms present in the aromatic moiety of the **Cbz-Cor** structure. The corresponding distances are 3.60 and 2.60 Å, respectively, while the nitrogenous bases DA-05, DA-06, DT-07, DT-19, DT-20, and DC-21 interact via van der Waals forces with the **Cbz-Cor** structure within distances of 3.80, 1.40, 3.50, 3.00, 3.00, and 3.50 Å, respectively.

4. Conclusions

In this study, we explored the photophysical and photobiological properties of substituted corroles with varying peripheral heterocycle units at the meso-10-position (**Cbz-Cor**, **MetCbz-Cor**, **PTz-Cor**, and **PTzEt-Cor**). We evaluated both singlet and triplet excited states. Additionally, we assessed photobiological parameters such as $^1O_2$ generation and photostability, finding that these compounds show promise for use in photoinduced processes. Moreover, we examined the interactive properties of corroles with biomacromolecules, specifically DNA and HSA. Our findings suggest that the corrole derivatives preferentially interact in the minor grooves of DNA due to secondary forces, clearly evidenced in site III of the albumin.

CRediT authorship contribution statement

Bruna Matiuzzi Rodrigues: Methodology, Investigation, Formal analysis. **Diego Franca de Oliveira:** Methodology, Investigation, Formal analysis, Conceptualization. **Rafael de Queiroz Garcia:** Methodology, Investigation, Formal analysis, Conceptualization. **Otávio Augusto Chaves:** Writing – original draft, Methodology, Investigation, Formal analysis, Conceptualization. **Gabriela Faria Pizzi:** Methodology, Investigation, Formal analysis, Conceptualization. **Luiz Antônio Sodré Costa:** Writing – original draft, Validation, Supervision, Investigation. **Leonardo de Boni:** Writing – original draft, Validation, Supervision, Project administration, Funding acquisition, Conceptualization. **Bernardo Almeida Iglesias:** Writing – original draft, Visualization, Validation, Supervision, Project administration, Investigation, Funding acquisition, Conceptualization.

Declaration of competing interest

The authors declare no conflicts of interest.

Data availability

Data will be made available on request.

Acknowledgements

This study was financed by CNPq, CAPES, FAPESP and FAPERGS. Bernardo A. Iglesias thanks to Conselho Nacional de Desenvolvimento Cientíífico e Tecnológico (CNPq – Brazil; Universal process 409150/2018-5 and PG-2018 grants process 304711/2018-7) and Coordenacão de Aperfeiçoamento de Pessoal de Nível Superior - Brazil (CAPES) - Finance Code 001. Leonardo de Boni thanks to FAPESP 2016/20886-1, CNPq Universal process 404551/2016-0 and PG-2019 grants process 306045/2019-2. Otávio A. Chaves thanks Fundação para a Ciência e a Tecnologia (FCT – Portuguese Agency for Scientific Research) for his Ph. D. fellowship 2020.07504.BD. LASC thanks CNPq for the research grant 310365/2021-0. We would also like to thank Atlas Assessoria Linguística for language editing.

Appendix A. Supplementary data

Supplementary data to this article can be found online at https://doi.org/10.1016/j.ijbiomac.2024.131861.

References

[1] S. Nardis, F. Mandoj, M. Stefanelli, R. Paolesse, Metal complexes of corrole, Coord. Chem. Rev. 388 (2019) 360–405.
[2] J.H. Palmer, Transition metal Corrole coordination chemistry: a review focusing on electronic structural studies, Molecular electronic structures of transition metal complexes I (2012) 49–89.

[3] R.D. Teo, J.Y. Hwang, J. Termini, Z. Gross, H.B. Gray, Fighting cancer with corroles. Chem. Ver. 117 (2017) 2711–2729.
[4] A. Preuß, I. Saltsman, A. Mahammed, M. Pfitzner, I. Goldberg, Z. Gross, B. Röder, Photodynamic inactivation of mold fungi spores by newly developed charged corroles, J. Photochem. Photobiol B: Biology 133 (2014) 39–46.
[5] T.A. Cardote, J.F. Barata, C. Amador, E. Alves, M.G.P. Neves, J.A. Cavaleiro, A. Cunha, A. Almeida, M.A.F. Faustino, Evaluation of meso-substituted cationic corroles as potential antibacterial agents, An. Acad. Bras. Cienc. 90 (2018) 1175–1185.
[6] P.S. Lacerda, M. Bartolomeu, A.T. Gomes, A.S. Duarte, A. Almeida, M.A. Faustino, M.G. Neves, J.F. Barata, Can Corrole dimers be good photosensitizers to kill Bacteria? Microorganisms 10 (2022) 1167.
[7] W. Deng, M. Jia, Q. Shi, Y. Xu, Y. Feng, Y. Zhao, M. Gong, B. Zhang, A Unique Corrole-Based Metal–Organic Polymer for Synergistic Phototherapy, Mat. Chem, Front, 2024.
[8] X. Jiang, R.X. Liu, H.Y. Liu, C.K. Chang, Corrole-based photodynamic antitumor therapy, J. Chin. Chem. Soc. 66 (2019) 1090–1099.
[9] G. Lu, P. Zhang, Y. Fang, Y. Gao, Q. Hu, Synthesis, characterization and third order nonlinear optical properties of trans-A2B-type cobalt corroles, New J. Chem. 45 (2021) 2103–2109.
[10] P. Yadav, T. Anand, S.S.B. Moram, S. Bhattacharya, M. Sankar, S.V. Rao, Synthesis and femtosecond third order nonlinear optical properties of push-pull trans-A2B-corroles, Dyes & Pigm. 143 (2017) 324–330.
[11] B. Dozza, B.M. Rodrigues, I. Tisoco, V.B. de Souza, L. Angnes, B.A. Iglesias, Spectroelectrochemistry as a powerful technique for porphyrins/corroles derivatives electro-characterization: fundamentals and some examples, Microchem. J. 183 (2022) 108041.
[12] A. Varshney, D. Ahluwalia, R. Kubba, A. Kumar, Recent developments in corroles as an ion sensor, J. Indian Chem. Soc. 99 (2022) 100708.
[13] L. Tortora, G. Pomarico, S. Nardis, E. Martinelli, A. Catini, A. D'Amico, C. Di Natale, R. Paolesse, Supramolecular sensing mechanism of corrole thin films, Sens. Actuators B Chem. 187 (2013) 72–77.
[14] J.F. Barata, M.G.P. Neves, A.C. Tomé, M.A.F. Faustino, A.M. Silva, J.A. Cavaleiro, How light affects 5,10,15-tris(pentafluorophenyl)corrole, Tetrahedron Lett. 51 (2010) 1537–1540.
[15] A. Mahammed, Z. Gross, Corroles as triplet photosensitizers, Coord. Chem. Rev. 379 (2019) 121–132.
[16] L.G. Liu, Y.M. Sun, Z.Y. Liu, Y.H. Liao, L. Zeng, Y. Ye, H.Y. Liu, Halogenated gallium corroles: DNA interaction and photodynamic antitumor activity, Inorg. Chem. 60 (2021) 2234–2245.
[17] T.V. Acunha, O.A. Chaves, B.A. Iglesias, Fluorescent pyrene moiety in fluorinated C6F5-corroles increases the interaction with HSA and CT-DNA, J. Porphyr. Phthalocyanines 25 (2021) 75–94.
[18] T.V. Acunha, H.F. Victória, K. Krambrock, A.C. Marques, L.A.S. Costa, B.A. Iglesias, Photophysical and electrochemical properties of two trans-A2B-corroles: differences between phenyl or pyrenyl groups at the meso-10 position, Phys. Chem. Chem. Phys. 22 (2020) 16965–16977.
[19] B.M. Rodrigues, C.C. Diniz, V.N. da Rocha, M.H. Köhler, G.P. Brandão, L. A. Machado, E.N. da Silva Júnior, B.A. Iglesias, First report of trans-A2B-corrole derived from a lapachone derivative: photophysical, TD-DFT and photobiological assays. RSC advances 13 (2023) 11121–11129.
[20] A. Das, T.P. Mohammed, R. Kumar, S. Bhunia, M. Sankaralingam, Carbazole appended trans-dicationic pyridinium porphyrin finds supremacy in DNA binding/photocleavage over a non-carbazolyl analogue, Dalton Trans. 51 (2022) 12453–12466.
[21] P. Xu, L. Yuan, K. Wang, B. Pan, Y. Ye, K. Lu, Interaction of bifunctional peptide-carbazole complexes with DNA and antimicrobial activity, Int. J. Biol. Macromol. 237 (2023) 124070.
[22] A. Kumar, C. Vigato, D. Boschi, M.L. Lolli, D. Kumar, Phenothiazines as anti-cancer agents: SAR overview and synthetic strategies, Eur. J. Med. Chem. 254 (2023) 115337.
[23] W.B. Shao, R.S. Luo, J. Meng, X.K. Lv, H.M. Xiang, W.L. Xiao, X. Zhou, L.W. Liu, Z. B. Wu, S. Yang, Engineering phenothiazine-based functional mimics of host defense peptides as new agrochemical candidates: design, synthesis, and antibacterial evaluation, J. Agric. Food Chem. 71 (2023) 16950–16961.
[24] Jaipal Kandhadi, Wei-Cong Yan, Fan Cheng, Hui Wang, Hai-Yang Liu, Trans-A2B-corrole bearing 2,3-di(2-pyridyl)quinoxaline (DPQ)/phenothiazine moieties: synthesis, characterization, electrochemistry and photophysics, New J. Chem. 42 (2018) 9987–9999.
[25] B. Shivaprasadachary, A.R. Ramya, G. Reddy, L. Giribabu, Light induced intramolecular energy and electron transfer events in carbazole–corrole and phenothiazine-corrole dyads, J. Porphyr. Phthalocyanines 24 (2020) 693–704.
[26] R.R. Gagne, C.A. Koval, G.C. Lisensky, Inorg. Chem. 19 (1980) 2854–2855.
[27] A.M. Brouwer, Standards for photoluminescence quantum yield measurements in solution (IUPAC technical report), Pure Appl. Chem. 83 (2011) 2213–2228.
[28] L. De Boni, C. Toro, F.E. Hernandez, Excited state absorption study in hematoporphyrin IX, J. Fluoresc. 20 (2010) 197–202.
[29] D.C. Jornada, R. de Queiroz Garcia, C.H. da Silveira, L. Misoguti, C.R. Mendonca, R.C.V. Santos, L. De Boni, B.A. Iglesias, Investigation of the triplet excited state and application of cationic meso-tetra(cisplatin)porphyrins in antimicrobial photodynamic therapy, Photodiagnosis Photodyn. Ther. 35 (2021) 102459.
[30] B.M. Rodrigues, H.F. Victória, G. Leite, K. Krambrock, O.A. Chaves, D.F. de Oliveira, R.D.Q. Garcia, L. De Boni, L.A. Costa, B.A. Iglesias, Photophysical, photobiological, and biomolecule-binding properties of new tri-cationic meso-tri (2-thienyl)corroles with Pt(II) and Pd(II) polypyridyl derivatives, J. Inorg. Biochem. 242 (2023) 112149.
[31] B. Valeur, M.N. Berberan-Santos, Molecular Fluorescence: Principles and Applications, John Wiley & Sons, 2012.
[32] V.E. Korobov, V.V. Shubin, A.K. Chibisov, Triplet state of rhodamine dyes and its role in production of intermediates, Chem. Phys. Lett. 45 (1977) 498–501.
[33] A.D. Becke, Density-functional thermochemistry. III., The role of exact exchange, J. Chem. Phys. 98 (1993) 5648–5652.
[34] F. Weigend, R. Ahlrichs, Balanced basis sets of split valence, triple zeta valence and quadruple zeta valence quality for H to Rn: design and assessment of accuracy, Phys. Chem. Chem. Phys. 7 (2005) 3297–3305.
[35] S. Grimme, J. Antony, S. Ehrlich, H. Krieg, A consistent and accurate *ab initio* parametrization of density functional dispersion correction (DFT-D) for the 94 elements H-Pu, J. Chem. Phys. 132 (2010) 154104.
[36] S. Grimme, S. Ehrlich, L. Goerigk, Effect of the damping function in dispersion corrected density functional theory, J. Comput. Chem. 32 (2011) 1456–1465.
[37] J. Tomasi, B. Mennucci, R. Cammi, Quantum mechanical continuum solvation models, Chem. Rev. 105 (2005) 2999–3094.
[38] C. Adamo, D. Jacquemin, The calculations of excited-state properties with time-dependent Density functional theory, Chem. Soc. Rev. 42 (2013) 845–856.
[39] C. Adamo, V. Barone, Exchange functionals with improved long-range behavior and adiabatic connection methods without adjustable parameters: the m PW and m PW1PW models, J. Chem. Phys. 108 (1998) 664–675.
[40] F. Neese, The ORCA program system, Wiley Interdiscip. Rev.: Comput. Mol. Sci. 2 (2012) 73–78.
[41] F. Neese, Software update: the ORCA program system, version 4.0. Wiley interdisciplinary reviews: computational molecular, Science 8 (2018) e1327.
[42] R.C. Pivetta, B.L. Auras, B. de Souza, A. Neves, F.S. Nunes, L.H. Cocca, L. De Boni, B.A. Iglesias, Synthesis, photophysical properties and spectroelectrochemical characterization of 10-(4-methyl-bipyridyl)-5,15-(pentafluorophenyl) corrole, J. Photochem. Photobiol. A Chem. 332 (2017) 306–315.
[43] L.P. Fioravanço, J.B. Pòrto, F.M. Martins, J.D. Siqueira, B.A. Iglesias, B. M. Rodrigues, O.A. Chaves, D.F. Back, A vanadium (V) complexes derived from pyridoxal/salicylaldehyde. Interaction with CT-DNA/HSA, and molecular docking assessments, J. Inorg. Biochem. 239 (2023) 112070.
[44] T.V. Acunha, B.M. Rodrigues, J.A. da Silva, D.D. Galindo, O.A. Chaves, V.N. da Rocha, P.C. Piquini, M.H. Köhler, L. De Boni, B.A. Iglesias, Unveiling the photophysical, biomolecule binding and photo-oxidative capacity of novel Ru (II)-polypyridyl corroles: a multipronged approach, J. Mol. Liq. 340 (2021) 117223.
[45] I. Tisoco, M.C. Donatoni, H.F. Victória, J.R. de Toledo, K. Krambrock, O.A. Chaves, K.T. de Oliveira, B.A. Iglesias, Photophysical, photooxidation, and biomolecule-interaction of meso-tetra(thienyl) porphyrins containing peripheral Pt(II) and Pd (II) complexes. Insights for photodynamic therapy applications, Dalton Trans. 51 (2022) 1646–1657.
[46] H.R. Drew, R.M. Wing, T. Takano, C. Broka, S. Tanaka, K. Itakura, R.E. Dickerson, Proc. Natl. Acad. Sci. U. S. A. 78 (1981) 2179.
[47] M. Wardell, Z. Wang, J.X. Ho, J. Robert, F. Rucker, J. Ruble, D.C. Carter, The atomic structure of human Methemalbumin at 1.9 Å, Biochem. Biophys. Res. Commun. 291 (2002) 813–819.
[48] https://www.wavefun.com/, accessed in November 2023.
[49] http://www.ccdc.cam.ac.uk/solutions/csd-discovery/components/gold/, accessed in November 2023.
[50] T. Bessega, O.A. Chaves, F.M. Martins, T.V. Acunha, D.F. Back, B.A. Iglesias, G. M. de Oliveira, Inorg. Chim. Acta 496 (2019) 119049.
[51] V.A. Oliveira, H. Terenzi, L.B. Menezes, O.A. Chaves, B.A. Iglesias, J. Photochem. Photobiol. B 211 (2020) 111991.
[52] O.A. Chaves, L.B. Menezes, B.A. Iglesias, J. Mol. Liq. 294 (2019) 111581.
[53] O.A. Chaves, M.R.L. Santos, M.C.C. de Oliveira, C.M.R. Sant'Anna, R.C. Ferreira, A. Echevarria, J.C. Netto-Ferreira, J. Mol. Liq. 254 (2018) 280–290.
[54] DeLano, W. L.; PyMOL User's Guide; DeLano Scientific LLC:San Carlos, CA, USA (2002).
[55] S. Zakavi, S. Hoseini, The absorption and fluorescence emission spectra of meso-tetra (aryl)porphyrin dications with weak and strong carboxylic acids: a comparative study, RSC Adv. 5 (2015) 106774–106786.
[56] R.L. Martin, Natural transition orbitals, J. Chem. Phys. 118 (2003) 4775–4777.
[57] Z. Meng, H. Xue, T. Wang, B. Chen, X. Dong, L. Yang, J. Dai, X. Lou, F. Xia, Aggregation-induced emission photosensitizer-based photodynamic therapy in cancer: from chemical to clinical, J. Nanobiotechnology 20 (2022) 1–35.
[58] V.B. de Souza, V.N. da Rocha, P.C. Piquini, O.A. Chaves, B.A. Iglesias, Effects of substituents on the Photophysical/Photobiological properties of mono-substituted Corroles, Molecules 28 (2023) 1385.
[59] J.R. Lakowicz, Principles of Fluorescence Spectroscopy, 1st ed., Springer, New York, NY, USA, 2006.
[60] V. Viecelli, O.A. Chaves, K. Araki, P.R. Martins, B.A. Iglesias, J. Braz. Chem. Soc. 31 (2020) 2282–2298.
[61] O.A. Chaves, T.V. Acunha, B.A. Iglesias, C.S.H. Jesus, C. Serpa, J. Mol. Liq. 301 (2020) 112466.